Plasma-assisted catalysis of ammonia using tungsten at low pressures: a parametric study

Rodrigo Antunes,*,† Roland Steiner,† Carlos Romero Muñiz,‡ Kunal Soni,† Laurent Marot,† and Ernst Meyer†

†*Department of Physics, University of Basel, Klingelbergstrasse 82, CH-4056 Basel, Switzerland*

‡*Department of Physical, Chemical and Natural Systems, Universidad Pablo de Olavide, Ctra. Utrera km. 1, E-41013, Seville Spain*

E-mail: rodrigo.antunes@unibas.ch

Phone: +41 (0)61 2673730

Abstract

The production of ammonia (NH_3) with low-pressure, radiofrequency plasmas is studied in this paper in a wide range of experimental conditions using tungsten as catalyst. The relative position of the tungsten foil in the pyrex tube was observed to dramatically impact the ammonia formation. By positioning the catalyst in the middle of the tube, the concentration of NH_3 peaked at 120 W with $\approx$ 20 mol% , while it decreased by more than a factor of 2 at 300 W. When the foil was placed close to the end of the tube, the production of NH_3 was rather stable beyond 120 W. These results provide a clear evidence of the surface's role on the local enhancement of the NH_3 formation rates. In the plasma volume, at some distance from the foil, the decomposition of NH_3 is the major occurring process and the decomposition rate increases with the power primarily due to a higher electron density. The optimum production of NH_3 was

found to be at 45 mol% N_2 and 120 W, and the position of the maximum was observed to slightly decrease to < 40 mol% N_2 with an RF power of 60 W, highlighting that not only the material characteristics play a role but also the discharge conditions. The measured NH_3 decreased by increasing the pressure from 3 to 5 Pa, which is associated with a decrease in the electron temperature. The temperature of the discharge was found to have a negligible effect on NH_3 formation up 673 K, demonstrating one of the key features of plasma-catalysis in respect to thermal catalysis. The largest energy yield of 0.075 g-NH_3 kWh^{-1} was obtained with an equimolar mixture of N_2-H_2 at 30 W and 3 Pa. Overall, our results show that the changes in the electron density, electron temperature and gas composition allow a more effective tuning of the catalytic properties of tungsten than varying the bulk gas temperature.

Keywords

Plasma-assisted catalysis, ammonia, tungsten, low-pressure plasma, radiofrequency plasma

Introduction

Ammonia (NH_3) is currently produced at large scales *via* the well-known Haber-Bosch process, which was patented in 1909 and implemented industrially for the first time by BASF in 1913.[1] The destruction of the strong triple bond of N_2 is the main limiting step for the formation of NH_3, which can only take place at high temperatures ($650 - 700$ K).[2] However, since $3\,H_2 + N_2 \rightarrow 2\,NH_3$ is exothermic (-91.4 kJ mol^{-1}), the mere increase of temperature would reduce the ammonia concentration.[3] Therefore, higher pressures (≈ 200 bar) and an iron-based catalyst are necessary to ensure the feasibility of the process. Due to its high energy requirements and high demand for ammonia consumption, the worldwide production of NH_3 accounts for 1 to 2 % of the greenhouse gas emissions (although a large fraction of it is due to the production of H_2 from methane reforming).[4,5] Therefore, several alternative

paths for ammonia synthesis have been pursued.[6]

Plasma-assisted catalysis is one of the main techniques studied at laboratory scale to optimize the production of ammonia, which explores the interaction between low-temperature plasmas (LTPs) of N_2-H_2 and catalytic surfaces. In these plasmas most of the electrical energy is transferred *via* the electrons to the heavy species. Due to their low mass and heat capacity, even small amounts of energy in the electron gas lead to high electron temperatures (typically in the range of $1-10\,\mathrm{eV}$). In contrast, the heavy species remain at relatively low temperatures. In contrast to the conventional thermal synthesis of ammonia, the low gas temperatures in non-thermal plasmas favor the exothermic reaction at low-to-ambient pressures.[7] A thorough review of the plasma-catalysis literature for NH_3 synthesis has been recently published.[8] Several types of plasma discharges have been used for this purpose, e.g. dielectric barrier discharges (DBDs),[9–11] glow-discharge,[12] microwave[13,14] and radio-frequency[15,16] plasmas or linear plasma devices.[17] Much research has been devoted to understand the dissociation mechanisms of the N_2 molecule,[18–20] whose energy threshold of $9.8\,\mathrm{eV}$ contrasts to that of H_2 ($4.5\,\mathrm{eV}$).[21,22] The dominant dissociation mechanisms depend on the discharge conditions. At pressures below $10^2\,\mathrm{Pa}$, electron impact dissociation ($N_2 + e^- \rightarrow 2\,N + e^-$) is the major channel due to the high-energy electrons present in the tail of the electron energy distribution function. At larger pressures the production of atomic N *via* reactions among vibrationally excited N_2 molecules becomes important as wel.[19] In the presence of H_2, other dissociation channels are available, such as $HN_2^+ + e^- \rightarrow NH + N$, which takes place after the formation of HN_2^+ *via* charge transfer reactions, e.g. $N_2^+ + H_2 \rightarrow HN_2^+ + H$.[20]

In many studies the plasma is ignited inside a glass (pyrex or quartz) tube, which is already sufficient to produce ammonia in measurable amounts. Early studies reported the formation and decomposition of NH_3 produced inside such chambers.[23–26] The formation rate was found to be highly dependent on the inlet N_2-H_2 concentration, plasma power, gas flow and pressure. The catalytic activity increases further when metallic catalysts are immersed in the glow or afterglow regions, which highlights the importance of surface reac-

tions. The role of plasma-wall interactions for the production and loss of atomic H and N and NH_x species was identified by Gordiets *et al.* in early numerical models.[27,28] More recent numerical efforts identified the main production and loss channels of H, N and NH_x in low-pressure and atmospheric plasmas.[29–31] In both pressure ranges, a large fraction of atomic N is produced *via* electron-impact dissociation of N_2. At atmospheric pressures, atomic H is found to be produced either by electron-impact dissociation of NH_3 or *via* reactions involving molecular N_2. The latter seems to be the main source of H in low-pressure plasmas. The main loss channels of H and N involve heterogeneous surface processes, either to form new surface species (e.g., $N + H(s) \rightarrow NH(s)$) or by recombining back to their molecular form (e.g., $H + H(s) \rightarrow H_2$). There is currently a wide consensus in the literature that Langmuir-Hinshelwood (L-H) and/or Eley-Rideal (E-R) surface mechanisms largely contribute to the formation of NH_3. Their relative importance is however dependent on the plasma regime, gas temperature and reactivity of the surface.[4,32] The L-H mechanism, consisting of successive hydrogenation steps of adsorbed species (e.g., $H(s) + NH_2(s) \rightarrow NH_3$), requires high gas temperatures and highly reactive surfaces. On the other side, E-R, in which the hydrogenation takes place between adsorbed and gas phase species (e.g., $H + NH_2(s) \rightarrow NH_3$), becomes relevant at low gas temperatures and surfaces with a lower reactivity. Dominant destruction channels of NH_3 include electron-impact dissociation and heavy-species reactions.[15,30]

Venugopalan *et al.* showed that the catalytic activity increases with the electron work function W of the metals with a three-fold increase in NH_3 yield for platinum ($W_{Pt} = 5.5\,eV$) when compared to aluminium ($W_{Al} = 4.2\,eV$).[33] More recently, Iwamoto *et al.* have found that the NH_3 synthesis rate in atmospheric plasmas (with no external heating) decreases when the formation stability of metal nitrides increases.[34] They reported that the ammonia yield decreases in the following order: Au > Pd > Cu > Fe > W. These results are consistent to those published by Shah *et al.*, in which the catalytic activity was found to be highest for Au and lowest for Fe at 300 W of RF power at 34 Pa.[15] Moreover, Mehta *et al.* developed a microkinetic model to demonstrate the importance of the vibrationally

excited N_2 molecules which lower the dissociation barriers, hence increasing the ammonia yield.[35] Considering atmospheric pressures and elevated temperatures for the background gas (473 K) and population of the vibrationally excited molecules (3000 K), they showed that the so-called turnover frequency (TOF) depends on the N adsorption energy *via* a volcano-type plot. For vacuum plasmas, Shah and co-workers have recently reported that no correlation exists between the NH_3 yields and N adsorption energies.[36] Instead, the ammonia formation is limited by the balance of the energy barriers for three kinetic processes: H diffusion into the bulk ($E_{\mathrm{H}}^{\mathrm{diff}}$), H-H recombination and H-N formation *via* the so-called Eley-Rideal mechanism (with activation energies $E_{\mathrm{HH}}^{\mathrm{ER}}$ and $E_{\mathrm{NH}}^{\mathrm{ER}}$, respectively). The authors postulate that the good hydrogen sink properties (i.e., hydrogen dissolution) of the metals have a net effect of increasing NH_3 formation since it hinders the H recombination on the surface to form H_2. Using these parameters, the authors presented a volcano-type plot with the TOF vs $\Delta E \equiv E_{\mathrm{HH}}^{\mathrm{ER}} + E_{\mathrm{H}}^{\mathrm{diff}} - E_{\mathrm{NH}}^{\mathrm{ER}}$.

Ammonia is a by-product in fusion reactors as a result of the interaction between hydrogen isotopes, nitrogen and tungsten surfaces.[37,38] Since its occurrence is undesirable, it is important to understand the NH_3 formation mechanisms and find mitigation strategies. Therefore, our group started investigating the catalytic properties of tungsten using 13.56 MHz RF plasmas.[16,39] The main focus of these investigations was to study the impact of the inlet concentration and presence of Ar and He impurities on the ammonia yield inside a quartz chamber with a tungsten foil. The results showed an optimum performance at an equimolar of N_2-H_2, which can be reduced by adding He into the plasma. In contrast, Ar promotes further the increase of nitrogen active species (e.g., N^+) in the plasma volume, which contributes to a higher ammonia yield. The previous work did not investigate the role of the plasma power, pressure or temperature on the ammonia formation and subsequent destruction. Such study is required for a better understanding of the underlying volume and surface mechanisms responsible for ammonia formation or destruction in the presence of tungsten, which is a poorly studied material in the plasma-catalysis community. This work

discusses the results obtained from a wide parametric study carried out with low-pressure RF N_2-H_2 plasmas.

Experimental setup and procedure

Metal-free chamber

Our metal-free setup is described in detail elsewhere,[16] and therefore only a brief description is provided here. The schematic diagram of the setup is presented in Figure 1 (a photograph of the actual setup is shown in Figure S5). The inlet gases (H_2, N_2, Ar with 6.0 purity) are continuously supplied using either Mass Flow Controllers (MFCs, Brooks GF40) or a leak valve. The plasma source is an in-house developed surface wave (surfatron) based on the design of Moisan *et al.*[40] This source is combined with a 13.56 MHz radiofrequency (RF) generator, with an associated impedance matching box, with a maximum set power of 300 W (Hüttinger GmbH and Co KG, PFM 1500A). The surfatron is attached to a 1400 mm-long pyrex chamber. The pyrex tube is connected *via* a 2 mm-wide PEEK pinhole to a high-vacuum (HV) chamber through which the gas phase species are pumped away. Moreover, a Residual Gas Analyser (Stanford Research Systems, RGA 200) is installed inside this chamber to quantify the species exiting the pyrex tube. The pressure in the HV chamber is kept

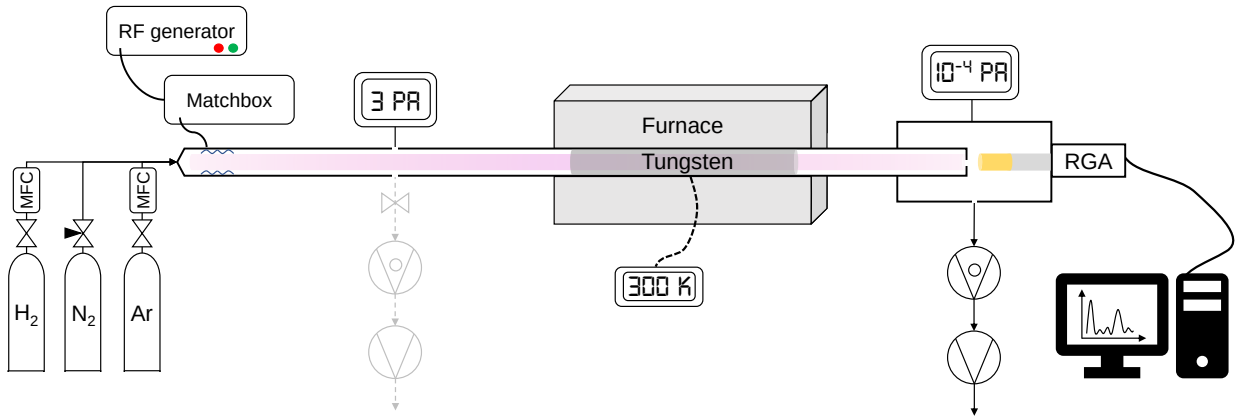

Figure 1: Schematic diagram of the experimental setup.

under 10^{-3} Pa during experiments, providing adequate pressures for the operation of the RGA and sufficiently high mean-free paths (on the order of 10 m) to avoid recombination of the dissociated species. The gas and plasma pressure (on the order of a few Pa during experiments) is measured with an MKS Baratron sensor mounted downstream of the source. The RGA is used to quantify the molar concentration of the gas species at the outlet of the pyrex chamber by measuring the mass-to-charge ratios m/z of the species of interest, i.e. $m/z = 2$ for H_2^+, $m/z = 17$ for NH_3^+ and $m/z = 28$ for N_2^+. The RGA is calibrated using the procedure presented in our previous paper[16] and periodic calibrations are performed to account for variations of the cracking patterns.

A tungsten foil (99.97 % 0.050 mm-thick, with an area of 500 cm^2 and with a roughness $R_a \approx 80$ nm, Plansee SE) was placed inside the pyrex tube and it was used for the catalytic studies presented below. Unless stated otherwise, all the results were obtained with the foil placed in the furnace region (Nabertherm GmbH), hence allowing experiments at high temperatures. To allow the oven to function during a plasma discharge, we applied a physically grounded shielding between the outer side of the tube glass and the inner part of the oven. A K-type thermocouple is installed on the outer surface of the pyrex tube to record an approximated temperature of the foil immediately after a discharge.

Typical run and experimental matrix

Before starting an experiment, the setup is evacuated down to background pressures below 10^{-2} Pa along the pyrex tube and below 2×10^{-6} Pa in the RGA chamber. Afterwards, the impurities remaining on the pyrex and tungsten surfaces are removed by argon cleaning, which consists in sputtering the walls with 120 W Ar plasma at around 0.6 Pa with ≈ 20 eV of ion energy for $1.5 - 2$ h (Figure S1). For each ammonia production experiment, an N_2-H_2 gas mixture is prepared by first injecting N_2 and then H_2 to ensure that the desired molar ratio is achieved. The plasma is then ignited during $10 - 15$ min, which is sufficient to achieve the steady-state for ammonia production. After stopping the discharge, the H_2

and N_2 flows are stopped. Each experiment is repeated at least once and the pressures, temperature and RGA signals are recorded throughout (a plot of a typical experiment is provided in Figure S2). Within the pressure range tested, the RGA signals increase linearly with the influx of particles present/formed in the pyrex tube.

Table 1: Summary of the experimental conditions.

RF power (W)	Pressure (Pa)	N_2 in H_2 (mol%)	Temperature (K)
$30 - 300$	3	50	300
120	$2 - 5$	50	300
120	3	$10 - 90$	300
120	3	50	$300 - 673$

A parametric study was carried out to investigate the influence of the plasma power, absolute pressure, inlet concentration and temperature (Table 1) on the ammonia molar concentration at steady-state, which is determined by equation (1) where p_i is the partial pressure of species i. The partial pressures are retrieved from the RGA signals following the procedure described in Ben-Yaala *et al.*[16] The energy yield associated with the ammonia synthesis is calculated using equation (2), where $M_{NH_3} \approx 17\,\mathrm{g\,mol^{-1}}$, F_{NH_3} is the NH_3 flow in $\mathrm{mol\,h^{-1}}$, P is the inlet power and $\eta = 0.5$ is the electrical efficiency of the RF generator, which remains constant at all powers.

$$X_{NH_3}(\%) = 100 \times \frac{p_{NH_3}}{p_{NH_3} + p_{N_2} + p_{H_2}} \tag{1}$$

$$E_{\mathrm{yield}}(\text{g-NH}_3\,\mathrm{kWh^{-1}}) = M_{NH_3} \times \frac{F_{NH_3}}{P/\eta} \tag{2}$$

The typical total flow used in the experiments was set to be around 1 sccm, where sccm stands for $\mathrm{cm^3\,min^{-1}}$ at standard conditions of temperature and pressure. In the whole studied range, the electron density n_e and electron temperature T_e were also determined using a commercial Langmuir probe (Hiden ESPion$^{\mathrm{TM}}$) placed at $\approx 600\,\mathrm{mm}$ from the source.

The plasma characterization results are presented in Figure S6.

All results presented below, except those obtained with the temperature excursion, were conducted with the furnace off. Nevertheless, due to the thermal heating of the pyrex tube during plasma discharges, the temperature on the outer side of the tube was measured to be in the range $308-373\,\mathrm{K}$ immediately after each run (with the highest temperature registered for $300\,\mathrm{W}$).

Results and discussion

Stability of ammonia production with tungsten

The stability of NH_3 over the tungsten foil was first studied by repeated discharges of an equimolar mixture of N_2-H_2 at $3\,\mathrm{Pa}$ and $120\,\mathrm{W}$. Figure 2 shows the raw data of the major peaks in the RGA spectrum. For approximately $3\,\mathrm{h}$ of plasma exposure along 5 cycles the amount of NH_3 was fairly constant. The constancy with tungsten has been also reported by Iwamoto *et al.*[34] using atmospheric plasmas. In this work, they observed an increase of the

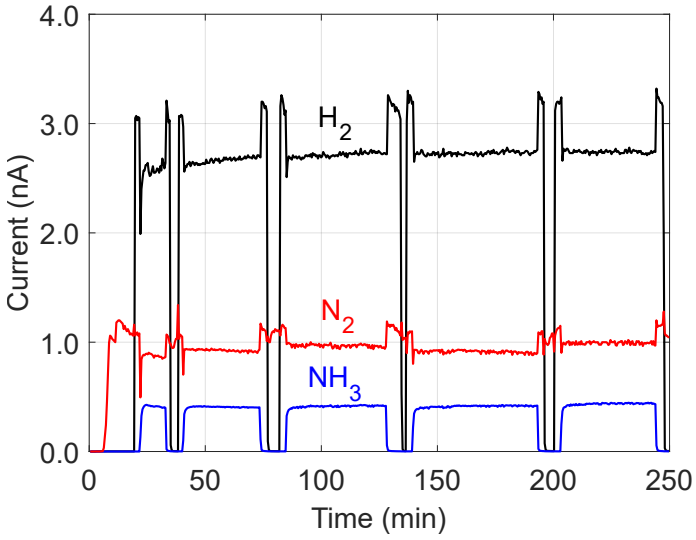

Figure 2: RGA signals for H_2, N_2 and NH_3 species as a function of the time for the stability experiment. Obtained for: $3\,\mathrm{Pa}$, $120\,\mathrm{W}$ and $50-50\,\mathrm{mol\%}$.

NH_3 production with the number of runs with palladium, silver or copper. They explained the results with the metallic deposits on the silica walls, which played a catalytic role.

It should be mentioned that the catalytic activity of tungsten remained unaltered when different W foils (from the same supplier) were employed. We have observed a decrease in the ammonia formation after a sequence of several experiments at different conditions, e.g. power or temperature. Nevertheless, Ar cleaning showed to be an effective way to recover the foil properties.

Influence of plasma power

For 3 Pa and $50 - 50$ mol%, the ammonia concentration was determined for $30 - 300$ W of input power, with and without the tungsten foil. The reflected power as given by the plasma generator was not higher than 2 W at all times. Figure 3a) shows that, without the tungsten foil, the input power has a slight positive impact on the production of ammonia. However, in the presence of the catalyst, the power strongly affects the amount of generated ammonia. In the range 30−120 W, the concentration of NH_3 in the outlet stream is doubled from 10 to 20 mol%. However, for 120−300 W, X_{NH_3} steadily decreases down to ≈ 7.5 mol%.

A larger input power corresponds to an increase of the plasma ionization, as confirmed by the Langmuir probe measurements of the electron density n_e (Figure S6). n_e was found to increase by a factor of 18 from 30 to 300 W. Therefore, higher dissociation and ionization rates of the major species are expected, hence increasing the amount of atomic H and N in the plasma volume. As result, a higher concentration of these species can participate in the formation of NH(s), which is an important precursor of NH_3. The formation of NH(s) has been described to be a result of Eley-Rideal reactions, given by (R1) and (R2) and/or Langmuir-Hinshelwood surface reaction (R3).[31] Other authors have reported the positive effect of the increased input power on the ammonia production.[15,41–44] For instance, S. Liu *et al.* reported a linear increase of NH_3 flow up to 60 W in a DBD discharge using a Ru/α-Al_2O_3 catalyst, whereas Shah *et al.* observed an increase of ammonia yield from 50 to 300 W

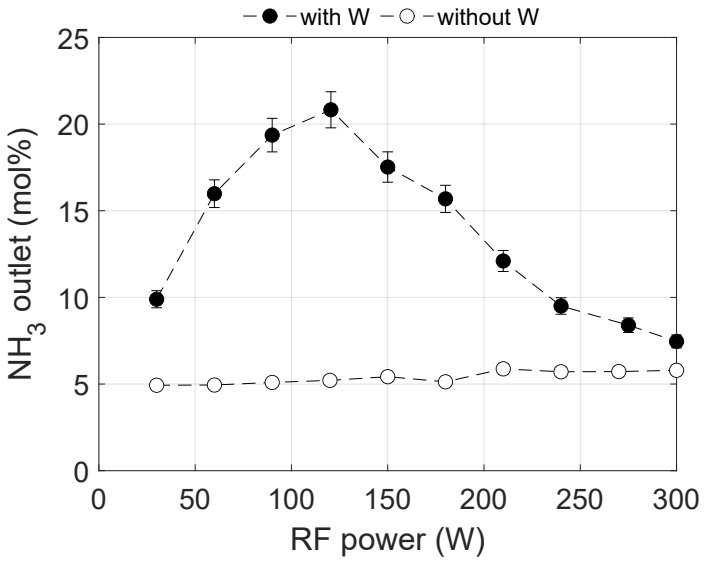

Figure 3: $X_{\mathrm{NH_3}}$ as a function of the RF power. Empty circles: without tungsten, filled circles: with tungsten.

with different transition metal wires using RF plasmas at 34 Pa and 673 K.[15]

$$\mathrm{N + H(s) \rightarrow NH(s)} \tag{R1}$$

$$\mathrm{H + N(s) \rightarrow NH(s)} \tag{R2}$$

$$\mathrm{H(s) + N(s) \rightarrow NH(s)} \tag{R3}$$

The particular profile for $X_{\mathrm{NH_3}}$ in Figure 3 shall be discussed in respect to the geometry of our setup. Between 30 and 300 W the plasma column length varied considerably, which is a typical feature of low pressure, surface-wave driven plasmas.[45] The plasma length increased from 30 to 120 W and it coincided roughly with the end of the catalyst foil for the latter. A further increase of the power led to an extension of the plasma until the end of the pyrex tube (Figure S7). As a result, the ammonia formed in the catalyst region might have been destroyed afterwards *via* electron-impact ionization, e.g. through (R4). The increase of n_e beyond 120 W until 300 W (by almost a factor of 2) increases the probability of electron

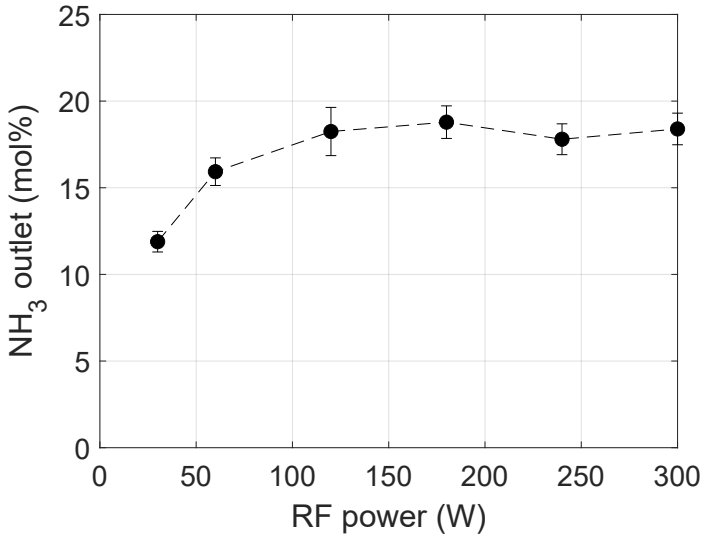

Figure 4: X_{NH_3} as a function of the input plasma power for position 2.

impact dissociation of NH_3, NH_2 and NH after the tungsten foil.

$$NH_3 + e^- \rightarrow NH + H_2 + e^- \tag{R4}$$

To test whether NH_3 is decomposed after the W foil, we performed another set of experiments by placing a new tungsten foil (with the same dimensions) shifted ≈ 300 mm towards the RGA chamber. At this position, only ≈ 50 mm of pyrex are left uncovered by the foil, which contrasts with ≈ 350 mm at position 1 (Figure S7). Figure 4 displays the obtained results, whereby the saturation of ammonia production is evident beyond 120 W. These results suggest that NH_3 is decomposed after the foil when placed at position 1. We further tested this hypothesis by injecting into the reactor high-purity NH_3. Upon a plasma discharge with a power as low as 10 W, we observed high conversion rates of ammonia ($> 80\%$) directly at the outlet of the surfatron. Similar results on the importance of placing the catalyst at the end of the plasma reactor to maximize the NH_3 formation have been recently reported by Yamijala *et al.*[46]

The main NH_3 loss mechanisms identified in the literature of low-temperature plasmas include the electron-impact dissociation and heavy-species reactions presented in (R4)-

(R8).[15,29,31] Consequently, we expect to see an increase in the signals of NH, NH_2, NH_4^+, H_2 and N_2 for position 1 beyond 120 W. The ratio NH_3/NH_2 remains constant for all experiments done in this work, indicating that the signal $m/z = 16$ of NH_2 is due to the cracking of NH_3 ($m/z = 17$) at the RGA. However, we do observe a decrease of NH_3/NH and NH_3/NH_4^+ with the increase of power (Figure S8), albeit the relative intensities of NH and NH_4^+ remain below 2% for all powers (Figure S4). While an increase in NH is expected for a larger n_e, the formation of NH_4^+ requires the presence of N_2H^+, whose relative intensity is around 1%. Furthermore, these trends are observed with and without the tungsten foil, and thus their presence alone cannot account for the destruction of NH_3. A possible explanation is the further decomposition of these species, e.g. $NH + e^- \rightarrow N + H + e^-$ and $NH_4^+ + \text{wall} \rightarrow NH_3 + H$, until the end of the reactor chamber. Instead, the RGA signals of H_2 and N_2 (and thus their concentrations) were lowest for 120 W with the foil at position 1, while they remained fairly constant with the foil positioned at the end of the reactor. Therefore, in our experiments NH_3 is observed to be converted back to its original precursors H_2 and N_2.

$$NH_3 + e^- \rightarrow NH_2 + H + e^- \tag{R5}$$

$$N_2H^+ + NH_3 \rightarrow NH_4^+ + N_2 \tag{R6}$$

$$N(D) + NH_3 \rightarrow NH_2 + NH \tag{R7}$$

$$NH_2 + e^- \rightarrow NH + H + e^- \tag{R8}$$

Influence of N_2-H_2 concentration

Figure 5 presents the steady-state ammonia concentration obtained for different inlet N_2 concentrations with and without catalyst. These results were obtained at a constant pressure of 3 Pa and carried out at 120 W (with and without catalyst) and 60 W (with catalyst). With no catalyst, a maximum of $X_{NH_3} \approx 6$ mol% in the range $\approx 30 - 50$ mol% N_2 is obtained. In

the presence of the tungsten surface, the X_{NH_3} profile is rather symmetric for 120 W, with ≈ 21 mol% as the highest attained concentration at $40-50$ mol% N_2, whereas for 60 W there is a slight shift of the maximum's position towards lower concentrations ($35-45$ mol% N_2). Moreover, the plasma column was shortest for 90 mol% N_2 and longest for 10 mol% N_2 (at which the plasma extended until the end of the pyrex tube, Figure S7). The increase of the plasma column for a larger H_2 content is explained by the lower ionization thresholds of both H_2 and H. Hence, the higher concentration of H^+, which does not recombine easily with electrons, contributes to an extension of the plasma with an associated decrease in the local power density. The higher presence of H_2 in the plasma volume also led to an increase of NH and NH_4^+ (Figure S9).

The smaller NH_3 production in H_2-rich plasmas is explained by the relatively higher presence of H species on the surface in comparison to N, hindering the formation of the ammonia precursor NH(s) (e.g., reactions (R1) and (R2)). By the same token, the presence of N_2 in large proportions is also detrimental to the formation of NH_3. Nevertheless, the shift in the optimum production from pyrex to tungsten is not straightforward. Several works have reported this effect with various materials.[9,28,34,44,47–54] In order to visualize the

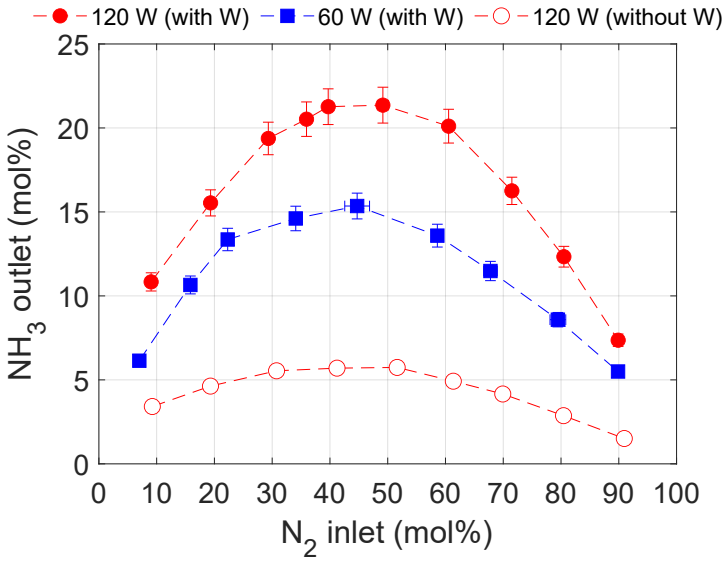

Figure 5: X_{NH_3} as a function of the inlet N_2 concentration for 120 W (red circles) and 60 W (blue squares). Empty circles: without tungsten, filled circles: with tungsten.

range of optimum N_2 reported in the literature, we fitted some of the published results using equation (3) for the reaction rate of NH_3,[55] where p_{H_2} and p_{N_2} are the partial pressures of H_2 and N_2, respectively, and k, α and β are fitting constants. The resulting normalized curves are presented in Figure 6 (refer to SI for information on the resulting fitting parameters).

$$r_{NH_3} = k p_{H_2}^{\alpha} p_{N_2}^{\beta} \tag{3}$$

Quartz, pyrex and $BaTiO_3$ provide an optimum production in the range $X_{N_2} = 34 - 40\,\text{mol}\%$, which is higher than the stoichiometric ratio of 1:3 N_2:H_2 in the conventional NH_3 synthesis process. The need for higher N_2 concentrations has been attributed to its high dissociation energy.[48] Thus, a higher amount of N_2 is needed to increase the probability of dissociation. However, an optimum production value for 1:4 N_2:H_2 was reported for $\alpha-Al_2O_3$ using DBD plasmas (not shown in the figure).[41] Furthermore, Body *et al.* reported an optimized production of ammonia around 40 mol% N_2 with their stainless steel setup using an RF magnetized plasma at low pressures,[54] which is quite consistent with previous results

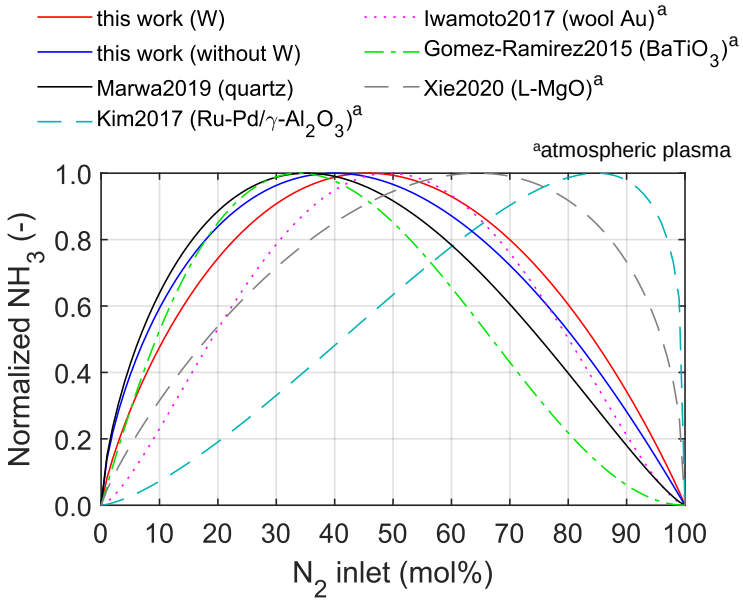

Figure 6: Normalized concentration of NH_3 as a function of the inlet N_2 concentration for results reported in the literature.

from our group.[39] In contrast, Ru-based catalysts require a N_2-rich environment, which may be explained by the poisoning of molecular and atomic hydrogen at high concentrations and pressures.[44,53,56] The low bulk density L-MgO catalyst is another example of a catalyst whose NH_3 production peaks at relatively high N_2 concentrations.[44] A recent work, combining electrochemical production of H_2 with N_2 RF plasmas, reported a small shift of the optimal production of NH_3 with a porous platinum catalyst.[57]

The position of the maximum for the various materials is difficult to rationalize without detailed mechanistic, microkinetic studies. Indeed, we could not find a correlation between the surface properties of transition metals (e.g., adsorption energy of N or H, calculated with DFT) and the NH_3 optimum position reported in the literature for W, Cu, Au, Ru. As discussed by Peng *et al.*,[58] the impact of the N_2-H_2 concentration on NH_3 formation may be also affected by the plasma characteristics (e.g., electron temperature and density) and discharge conditions.

Influence of absolute pressure

The impact of the absolute gas pressure on the production of ammonia is presented in Figure 7 for an equimolar mixture of N_2-H_2. The decrease of pressure from 5 to 3 Pa leads to an increase of X_{NH_3} and it eventually saturates between 3 and 2 Pa, with and without tungsten. The Langmuir probe measurements present a similar increase of T_e with the decrease of pressure (Table 2), and thus an increase of the reaction rates for electron-impact dissociation (and ionization) of N_2 and H_2 is expected.[29,31] The higher concentrations of atomic N and H may thus contribute to an increase of NH_3 on the surface. On the other side, the reaction rates for (R4), (R5) and (R8) will also increase (Table S2), which can explain the slight increase in the proportion of NH detected at lower pressures (Figure S9). The presence of NH_4^+ also seems to be enhanced at lower pressures, in contradiction with the observations from Carrasco *et al.* who reported an enhanced formation of NH_4^+ at higher p.[29] In their 10%-90% N_2-H_2 plasmas, N_2H^+ is an ion with a strong presence, and hence

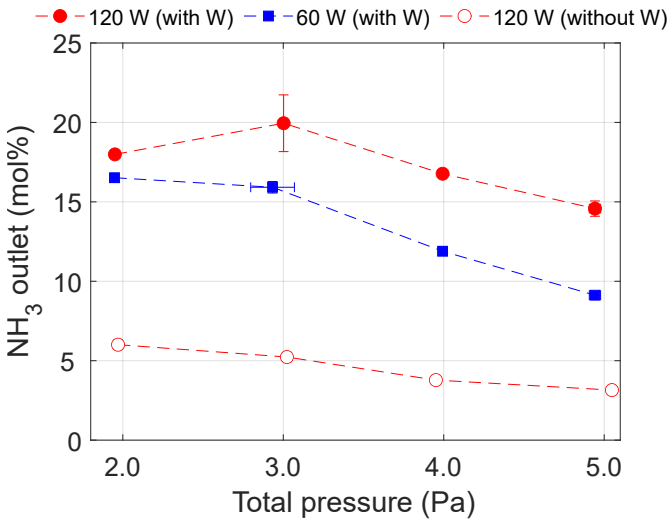

Figure 7: X_{NH_3} as a function of the absolute gas pressure for 120 W (red circles) and 60 W (blue squares) for an equimolar mixture of N_2-H_2. Empty circles: without tungsten, filled circles: with tungsten.

the relative rate of ion-neutral phase reaction (R8) increases when T_e is lower, which occurs at high pressures. It is worth mentioning that the extension of the plasma was observed to change with the pressure: while it receded about -100 mm from the end of the foil with $p = 3 \rightarrow 5$ Pa, the plasma column extended by $+300$ mm at 2 Pa (Figure S7). This behavior is well-known for surfatron discharges.[59,60]

The results should be further discussed in respect to the total inlet flow, which was increased from 0.65 to 1.88 sccm in order to increase the total pressure inside the pyrex chamber from 2 to 5 Pa. Consequently, the residence time of the precursors, estimated using equation (4) and given in Table 3, decreased with the increase of pressure. In our experiments, τ was around 2 to 4 times the values achieved in other works carried out at low pressures.[15,29]

Table 2: Electron density n_e and electron temperature T_e measured with Langmuir probe for different N_2-H_2 plasmas pressures generated with 120 W RF power and 50-50 mol% inlet concentration (see Supporting Information for detailed information).

p (Pa)	n_e (10^{10} cm^{-3})	T_e (eV)
2	4.78 ± 0.72	9.4 ± 1.4
3	4.56 ± 0.68	10.2 ± 1.5
4	3.16 ± 0.47	6.5 ± 1.0
5	2.92 ± 0.44	5.2 ± 0.8

Table 3: Estimated residence time τ for the pressure excursion experiments, using equation (4) where T_g is gas temperature, V and p the plasma volume and pressure, and F the molar flow of the gases at the inlet.

p (Pa)	$F_{H_2} + F_{N_2}$ (μmol s^{-1})	τ (s)
2	0.48	2.07
3	0.74	1.68
4	1.03	1.57
5	1.40	1.36

In Carrasco *et al.*, they show that the relative concentration of NH_3 increases by a factor of 1.5 from 8 to 0.8 Pa, despite a shorter residence time (0.75 to 0.45 s, respectively). These observations are attributed to an increase of T_e for lower p. Moreover, the range of T_e for which enhanced formation of NH_3 is achieved appears to be wider with the decrease of pressure. To the best of our knowledge, only one publication reports the impact of the residence time on NH_3 formation at low pressures.[61] In this work, Castro *et al.*. observed an increase in the NH_3 yield upon increasing τ from 50 to 100 ms. These results suggest that our residence times are sufficiently longer than the equilibration times required for the plasma-surface processes. Therefore, the higher X_{NH_3} for lower p is primarily attributed to the increase of T_e.

$$\tau = \frac{1}{RT_g} \frac{pV}{F_{H_2} + F_{N_2}} \tag{4}$$

Influence of the discharge temperature

We investigated further the impact of the temperature on NH_3 formation, and the results are displayed in Figure S10. A fairly constant yield was obtained up to 673 K at 120 W, whereas for 60 W a slight increase is obtained. Moreover, the signals ratios for NH_3/NH, NH_3/NH_2 and N/N_2 were also constant throughout. Nevertheless, a decrease of NH_3/NH_4 is observed for both powers at the highest temperatures, which is consistent with the increase of the plasma length as previously discussed.

The impact of temperature on ammonia formation has been mostly studied for atmospheric plasmas. Using DBD, Xie *et al.* reported a slight positive impact of the temperature on the production of ammonia for various catalysts.[44] This positive impact, also recently reported by L. R. Winter *et al.*,[62] is attributed to a combination of increased desorption of NH_3, that would have otherwise stayed on the surface, and enhanced reaction rates for the L-H mechanism. Several groups have identified L-H reactions involving N(s), H(s), NH(s) and NH_2(s) to contribute the most to NH_3 formation on the wall at low pressures.[15,29,31] Indeed, since L-H is an activated process, the reaction rate for ammonia formation is expected to increase at higher temperatures, provided the decomposition temperature is not exceeded (above 800 K for tungsten[39]). In our experiments, the NH_3 that is removed from the W surface (for instance during Ar cleaning after an H_2-N_2 experiment done at 300 K) is at least a factor of 10 less than the ammonia measured in the gas phase of N_2-H_2 plasmas. Hence, we expect the desorption of NH_3 at elevated temperatures to increase only slightly the NH_3 detected in gas phase. These results evidence the special features of low-temperature plasmas for the production of ammonia. Indeed, in thermal catalysis, the rate-limiting step is the dissociation of N_2, which must occur on the catalyst surface and strongly depends on T_g.[63] With LTPs, the plasma can be a reliable source of dissociated N, so that N_2 dissociative adsorption is no longer rate determining.[64]

Discussion

Our results show that the catalytic performances of W seem to be more effectively tuned by properties that directly affect n_e, T_e and plasma composition (through the plasma power, pressure and inlet N_2-H_2 mixture) rather than by increasing the bulk gas temperature. These observations are consistent with other experiments and modelling works carried out with atmospheric plasmas, whereby the plasma power has a stronger effect on the NH_3 yields than the temperature.[64,65]

Iwamoto *et al.* presented a reasonable correlation between NH_3 synthesis rate with the N adsorption energy with atmospheric plasmas.[34] They concluded that the highest performance for Au is related to the instability of the surface nitride, explained by its relatively weak tendency to adsorb N. To investigate whether a similar tendency could be obtained with vacuum plasmas, we carried out quantum calculations based on Density Functional Theory (DFT) to estimate the adsorption energies of N and H species on some representative metallic substrates. We have performed plane-wave calculations using the VASP package[66] with a cutoff energy of 400 eV, the PBE-D3[67,68] approach as exchange and correlation functional and projector augmented wave pseudopotentials.[69,70] The details of the procedure and calculated energies are presented in the Supporting Information. Figure 8 compares the energy yield per unit area of catalyst using the same materials at low and atmospheric pressures. A general increasing trend of the yield with a decrease in adsorption strength can be appreciated, although a stronger linear correlation ($R^2 \approx 0.61$) is obtained for the atmospheric plasmas. Interestingly, W, Fe, Cu and Ag seem to follow a linear increase with E_N^{ad} for both pressure regimes. As discussed by Shah *et al.*, in vacuum plasmas other parameters such as the activation barrier of H diffusion into the bulk or NH formation *via* E-R may have also to be considered for a more accurate description of the NH_3 formation processes.[36] Nevertheless, we could not reproduce the volcano plot presented in their paper, mainly due to differences in the N adsorption energies of Au and Ag (refer to Figure S11 and discussion therein). In their recent study, Yamijala *et al.* provide new insights on the mechanistic understanding of NH_3 synthesis at low pressures. They concluded that the pathways to NH_3 formation are distinct for both Cu and Pt (with $E_{N,Pt}^{ad} < E_{N,Cu}^{ad}$): in the former, the main interactions are between the plasma-phase atomic N and the H-terminated surface, whereas in the latter the surface must be saturated with NH. Similar plots to that of Figure 8 would be obtained for the adsorption of NH or NH_2 on the surface, in agreement with scaling relations, where $E_N^{ad} < E_{NH}^{ad} < E_{NH_2}^{ad}$[71] (see Supporting Information). The dissociative adsorption of vibrationally excited N_2 is also considered to have an important role even at low pressures, especially for

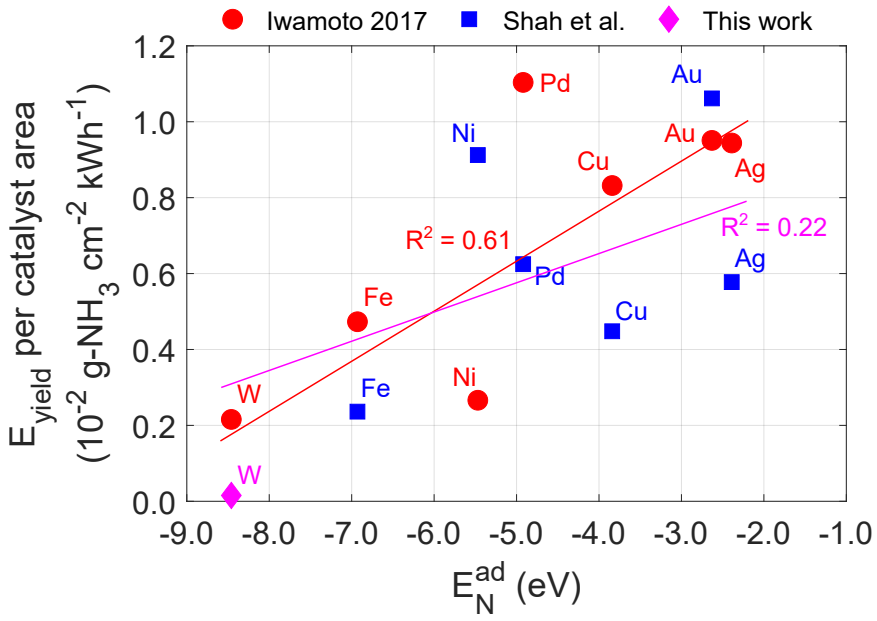

Figure 8: E_{yield} per unit area of catalyst obtained with various metals. Red circles obtained from Iwamoto *et al.* data,[34] blue squares obtained from Shah *et al.* data[15,36] and magenta diamond obtained from W in this work (using the highest $E_{yield} = 0.075\,\text{g-NH}_3\,\text{kWh}^{-1}$). The red fitting line was obtained using Iwamoto's data, whereas the magenta fitting line was determined using Shah's and our results.

surfaces with a high affinity to N.[46,64]

The RF power excursion experiments show that the decrease of NH_3 or its saturation beyond 120 W represents a waste of the input energy, as its increase does not translate into a higher production of ammonia. Furthermore, even though the amount of ammonia increases up to 120 W, the energy yield actually decreases: from 30 to 120 W, X_{NH_3} increases by a factor of 2, whereas the RF power increases by a factor of 4. The highest energy yield of $0.075\,\text{g-NH}_3\,\text{kWh}^{-1}$ was obtained for the lowest power of 30 W. This value is lower than the value obtained by Shah *et al.* with a gold mesh ($0.2\,\text{g}_{\text{NH}_3}\,\text{kWh}^{-1}$).[15] However, attention must be paid to the geometry of the setup, flows employed and type of discharge. Shah *et al.* used a setup with a reactor volume per catalyst area of $V/A = 0.275\,\text{cm}$, whereas $V/A \approx 2.6\,\text{cm}$ was maintained during our experiments. Moreover, the flow employed in Shah's experiments was at least a factor of 10 larger, and their discharge was generated inductively, with which a different coupling is expected when compared to the surfatron. The energy yields achieved

at low pressures are in stark contrast with those obtained with atmospheric plasmas, for which energy yields above $10\,g_{NH_3}\,kWh^{-1}$ have been reported.[53,72] The higher yields are nevertheless obtained at the expense of less concentrated streams ($10^2 - 10^3$ ppm instead of $> 10^5$ ppm for this work). This trade-off between energy yield and ammonia concentration for vacuum and atmospheric plasmas has been addressed in the literature.[4,15,73] One key distinctive factor that helps explaining it is the mass-flow employed, with typical values around 50 sccm for atmospheric plasmas,[65,74] corresponding to 50 times the throughputs used in our experiments. Consequently, a decrease of NH_3 yield by a factor of 10 can be well compensated by the large flows. Moreover, the power consumption of the vacuum pumps employed with low pressure plasmas should be also factored in for a more realistic figure. In the discussions above, only the plasma input power was used to allow a comparison with the work of Shah *et al.* Since we used both a primary pump and a turbopump (only to ensure the operation of the RGA), a further decrease by a factor of 10 in the E_{yield} is estimated (i.e., $E_{yield} \approx 0.0075\,g\text{-}NH_3\,kWh^{-1}$). On the other side, the low pressure plasmas allow for an uniformity of the reactants over the catalyst surface, hence leading to higher yields.[15] An important aspect as well is the ambient temperature of the background gas with low pressure plasmas, which favors the thermodynamic conversion of N_2 and H_2 into NH_3.

The need to bridge the gap between low-pressure and atmospheric plasmas is currently a major issue that needs to be addressed in the field of plasma-catalysis for NH_3 formation.[4] As discussed by Kim *et al.*,[75] the best yields achieved so far (in the range of $30\,g\text{-}NH_3\,kWh^{-1}$)[53] need to be raised by a factor of 10 to be competitive with the Haber-Bosch process.

Conclusions

In this work we present an exhaustive study of the catalytic activity of tungsten for ammonia formation using N_2-H_2 13.56 MHz RF plasmas. The work was carried out at a wide range of power, concentration, pressure and temperature. The production of NH_3 was found to be

highest at 120 W, 3 Pa and $50 - 50$ mol% N_2-H_2. We observed a significant impact of the plasma extension in relation to the tungsten foil position: the increase of the discharge length beyond the foil at large powers (approximately 350 mm of uncoveredy pyrex surface) led to an overall decrease of NH_3 by more than a factor of 2. However, when placed closer to the end of the pyrex tube (50 mm of uncoveredy pyrex surface), the produced ammonia remained constant with the increase of power. The use of the RGA alone did not allow verifying that NH_3 is being converted to NH or NH_4 in light of the main destruction mechanisms identified in the literature. The optimum production of NH_3 was observed to be in the range of $40 - 50$ mol% N_2 for 120 W. The position of the optimum production is not evident and cannot be explained by the material properties alone. The decrease of NH_3 production with the increase of pressure is attributed to an associated decrease in T_e. We also observed a constancy of NH_3 up to 673 K, which demonstrates that the use of LTPs with tungsten lifts the equilibrium-limit encountered in thermal catalysis.

Acknowledgement

The authors would like to thank the fruitful scientific discussions with Prof. Luís Lemos Alves, Prof. Vasco Guerra and Prof. Luís Marques. This work has been carried out within the framework of the EUROfusion Consortium and has received funding from the Euratom research and training programme 2014–2018 and 2019–2020 under grant agreement no. 633053. The views and opinions expressed herein do not necessarily reflect those of the European Commission or of the ITER Organization. ITER is the Nuclear Facility INB no. 174. This paper applies new physics analysis related to tritiated ammonia formation which is not yet incorporated into the ITER technical baseline. The nuclear operator is not constrained by the results presented here. The authors would like to thank the Swiss Federal Office of Energy, the Swiss Nanoscience Institute, the Swiss National Science Foundation and the Federal Office for Education and Science for their financial support.

Supporting Information Available

The following files are available free of charge.

- Antunes_ammonia_parametric_paper_SI.tex: complementary results and discussion on the origin ofpeaks 15, 18 and 29 in the RGA spectra, plasma characterization results with a Langmuir probe, plasma length variation with the experimental conditions and the two foil positions used in this work, additional data from the NH_3 production experiments, fitting parameters using the first-order kinetic equation and description of the DFT calculations.

References

(1) Tamaru, K. In *Catalytic Ammonia Synthesis: Fundamentals and Practice*; Jennings, J. R., Ed.; Springer, 1991; Chapter 1. The History of the Development of Ammonia Synthesis, p 15.

(2) Modak, J. M. Haber process for ammonia synthesis. *Resonance* **2002**, *16*, 69–77.

(3) Demirhan, C. D.; Tso, W. W.; Powell, J. B.; Pistikopoulos, E. N. Sustainable ammonia production through process synthesis and global optimization. *AIChE J.* **2019**, *65*, 1–23.

(4) Carreon, M. L. Plasma catalytic ammonia synthesis: state of the art and future directions. *J. Phys. D: Appl. Phys.* **2019**, *52*, 483001.

(5) Smith, C.; Hill, A. K.; Torrente-Murciano, L. Current and future role of Haber–Bosch ammonia in a carbon-free energy landscape. *Energy Environ. Sci.* **2020**, *13*, 331–344.

(6) Barboun, P. M.; Hicks, J. C. Unconventional Catalytic Approaches to Ammonia Synthesis. *Annu. Rev. Chem. Biomol. Eng.* **2020**, *11*, 5.1–5.19.

(7) Mizuno, A.; Craven, M. In *Plasma Catalysis*; Tu, X., Whitehead, J. C., Nozaki, T., Eds.; Springer, 2019; Chapter 2. Plasma Catalysis Systems, pp 21–24.

(8) Rouwenhorst, K. H. R.; Engelmann, Y.; van 't Veer, K.; Postma, R. S.; Bogaerts, A.; Lefferts, L. Plasma-driven catalysis: green ammonia synthesis with intermittent electricity. *Green Chem.* **2020**, *22*, 6258–6287.

(9) A. Gómez-Ramírez, J. C.; Lambert, R. M.; González-Elipe, A. R. Efficient synthesis of ammonia from N_2 and H_2 alone in a ferroelectric packed-bed DBD reactor. *Plasma Sources Sci. Technol.* **2015**, *24*, 065011.

(10) Wang, Y.; Craven, M.; Yu, X.; Ding, J.; Bryant, P.; Huang, J.; Tu, X. Plasma-Enhanced Catalytic Synthesis of Ammonia over a Ni/Al2O3 Catalyst at Near-Room Temperature: Insights into the Importance of the Catalyst Surface on the Reaction Mechanism. *ACS Catal.* **2019**, *9*, 10780–10793.

(11) Xie, Q.; Zhuge, S.; Song, X.; Lu, M.; Yu, F.; Ruan, R.; Nie, Y. Non-thermal atmospheric plasma synthesis of ammonia in a DBD reactor packed with various catalysts. *J. Phys. D: Appl. Phys.* **2020**, *53*, 064002.

(12) de Castro, A.; Tabarés, F. Role of nitrogen inventory and ion enhanced N-H recombination in the ammonia formation on tungsten walls. A DC glow discharge study. *Vacuum* **2018**, *151*, 66–72.

(13) Jauberteau, J. L.; Jauberteau, I.; Aubreton, J. NH_3 and $NH_{x<3}$ radicals synthesis downstream a microwave discharge sustained in an Ar–N_2–H_2 gas mixture. Study of surface reactive processes and determination of rate constants. *J. Phys. D: Appl. Phys.* **2002**, *35*, 665–674.

(14) Nakajima, J.; Sekiguchi, H. Synthesis of ammonia using microwave discharge at atmospheric pressure. *Thin Solid Films* **2008**, *516*, 4446–4451.

(15) Shah, J.; Wang, W.; Bogaerts, A.; Carreon, M. L. Ammonia Synthesis by Radio Frequency Plasma Catalysis: Revealing the Underlying Mechanisms. *ACS Appl. Energy Mater.* **2018**, *1*, 4824–4839.

(16) Ben Yaala, M.; Saeedi, A.; Scherrer, D.-F.; Moser, L.; Steiner, R.; Zutter, M.; Oberkofler, M.; De Temmerman, G.; Marot, L.; Meyer, E. Plasma-assisted catalytic formation of ammonia in N_2-H_2 plasma on a tungsten surface. *Phys. Chem. Chem. Phys.* **2019**, *21*, 16623–16633.

(17) Laguardia, L.; Caniello, R.; Cremona, A.; Dellasega, D.; Dell'Era, F.; Ghezzi, F.; Gittini, G.; Granucci, G.; Mellera, V.; Minelli, D.; Pallotta, F.; Passoni, M.; Ricci, D.; Vassallo, E. Ammonia formation and W coatings interaction with deuterium/nitrogen plasmas in the linear device GyM. *J. Nucl. Mater.* **2015**, *463*, 680–683.

(18) Ferreira, C. M.; Tatarova, E.; Guerra, V.; Gordiets, B. F.; Henriques, J.; Dias, F. M.; Pinheiro, M. Modeling of Wave Driven Molecular (H_2, N_2, N_2–Ar) Discharges as Atomic Sources. *IEEE Trans. Plasma Sci.* **2003**, *31*, 645–658.

(19) Guerra, V.; Sá, P. A.; Loureiro, J. Kinetic modeling of low-pressure nitrogen discharges and post-discharges. *Eur. Phys. J. Appl. Phys.* **2004**, *28*, 125–152.

(20) Tatarova, E.; Guerra, V.; Henriques, J.; Ferreira, C. M. Nitrogen dissociation in low-pressure microwave plasmas. *J. Phys. Conf. Ser.* **2007**, *71*, 012010.

(21) Frost, D. C.; McDowell, C. A. The Dissociation Energy of the Nitrogen Molecule. *Proc. R. Soc. London A.* **1956**, *236*, 278–284.

(22) Gerzberzg, G. The dissociation energy of the hydrogen molecule. *J. Mol. Spectrosc.* **1970**, *33*, 147–168.

(23) d'Agostino, R.; Cramarossa, F.; De Benedictis, S.; Ferraro, G. Kinetic and Spectro-

scopic Analysis of NH_3 Decomposition Under R.F. Plasma at Moderate Pressures. *Plasma Chem. Plasma Process.* **1981**, *1*, 1981.

(24) Haruo, U.; Takeshi, U.; Hideaki, N.; Osamu, M. Synthesis of Ammonia with RF Discharge Adsorption of Products on Zeolite. *Chem. Lett.* **1987**, 555–587.

(25) Touvelle, M.; Muñoz Licea, J. L. . M. V. Plasma Chemical Synthesis. II. Effect of Wall Surface on the Synthesis of Ammonia. *Plasma Chem. Plasma Process.* **1987**, *7*, 101–108.

(26) Amorim, J.; Baravian, G.; Sultan, G. Absolute density measurements of ammonia synthetized in N_2–H_2 mixture discharges. *Appl. Phys. Lett.* **1996**, *68*, 1915–1917.

(27) Gordiets, B.; Ferreira, C. M.; Pinheiro, M. J.; Ricard, A. Self-consistent kinetic model of low-pressure N_2–H_2 flowing discharges: I. Volume processes. *Plasma Sources Sci. Technol.* **1998**, *7*, 363–378.

(28) Gordiets, B.; Ferreira, C. M.; Pinheiro, M. J.; Ricard, A. Self-consistent kinetic model of low-pressure N_2–H_2 flowing discharges: II. Surface processes and densities of N, H, NH_3 species. *Plasma Sources Sci. Technol.* **1998**, *7*, 379–388.

(29) Carrasco, E.; Jiménez-Redondo, M.; Tanarro, I.; Herrero, V. J. Neutral and ion chemistry in low pressure dc plasmas of H_2/N_2 mixtures: routes for the efficient production of NH_3 and NH_4^+. *Phys. Chem. Chem. Phys.* **2011**, *13*, 19561–19572.

(30) Hong, J.; Pancheshnyi, S.; Tam, E.; Lowke, J. J.; Prawer, S.; Murphy, A. B. Kinetic modelling of NH_3 production in N_2–H_2 non-equilibrium atmospheric-pressure plasma catalysis. *J. Phys. D: Appl. Phys* **2017**, *50*, 154005.

(31) Jiménez-Redondo, M.; Chatain, A.; Guaitella, O.; Cernogora, G.; Carrasco, N.; Lemos Alves, L.; Marques, L. N_2-H_2 capacitively coupled radio-frequency discharges

at low pressure. Part II. Modelling results: the relevance of plasma-surface interaction. *Plasma Sources Sci. Technol.* **2020**, *29*, 085023.

(32) Hong, J.; Prawer, S.; Murphy, A. B. Plasma Catalysis as an Alternative Route for Ammonia Production: Status, Mechanisms, and Prospects for Progress. *ACS Sustainable Chem. Eng.* **2018**, *6*, 15–31.

(33) Yin, K. S.; Venugopalan, M. Plasma Chemical Synthesis. I. Effect of Electrode Material on the Synthesis of Ammonia. *Plasma Chem. Plasma Process.* **1983**, *3*, 343–350.

(34) Iwamoto, M.; Akiyama, M.; Aihara, K.; Deguchi, T. Ammonia Synthesis on Wool-Like Au, Pt, Pd, Ag, or Cu Electrode Catalysts in Nonthermal Atmospheric-Pressure Plasma of N_2 and H_2. *ACS Catal.* **2017**, *7*, 6924–6929.

(35) Mehta, P.; Barboun, P.; Herrera, F. A.; Kim, J.; Rumbach, P.; Go, D. B.; Hicks, J. C.; Schneide, W. F. Overcoming ammonia synthesis scaling relations with plasma-enabled catalysis. *Nat. Catal.* **2018**, *1*, 269–275.

(36) Shah, J.; Gorky, F.; Psarras, P.; Seong, B.; Gómez-Gualdrón, D. A.; Carreon, M. L. Enhancement of the Yield of Ammonia by Hydrogen-Sink Effect during Plasma Catalysis. *ChemCatChem.* **2020**, *11*, 1–13.

(37) D. Neuwirth, T. S.-S., V. Rohde; the ASDEX Upgrade Team, Formation of ammonia during nitrogen-seeded discharges at Asdex Upgrade. *Plasma Phys. Controlled Fusion* **2012**, *54*, 085008.

(38) Kallenbach, A.; Bernert, M.; Dux, R.; Casali, L.; Eich, T.; Giannone, L.; Herrmann, A.; McDermott, R.; Mlynek, A.; Müller, H. W.; Reimold, F.; Schweinzer, J.; Sertoli, M.; Tardini, G.; Treutterer, W.; Viezzer, E.; Wenninger, R.; Wischmeier, M.; Upgrade Team, A. Impurity seeding for tokamak power exhaust: from present devices via ITER to DEMO. *Plasma Phys. Controlled Fusion* **2013**, *55*, 124041.

(39) Ben Yaala, M. B.; Scherrer, D.-F.; Saeedi, A.; Moser, L.; Soni, K.; Steiner, R.; De Temmerman, G.; Oberkofler, M.; Marot, L.; Meyer, E. Plasma-activated catalytic formation of ammonia from N_2–H_2: influence of temperature and noble gas addition. *Nucl. Fusion* **2020**, *60*, 016026.

(40) Moisan, M.; Zakrzewski, Z. Plasma sources based on the propagation of electromagnetic surface waves. *J. Phys D: Appl. Phys.* **1991**, *24*, 1025–1048.

(41) Bai, M.; Zhang, Z.; Bai, X.; Bai, M.; Ning, W. Plasma Synthesis of Ammonia With a Microgap Dielectric Barrier Discharge at Ambient Pressure. *IEEE Trans. Plasma Sci.* **2003**, *31*, 1285–1291.

(42) Akay, G.; Zhang, K. Process Intensification in Ammonia Synthesis Using Novel Coassembled Supported Microporous Catalysts Promoted by Nonthermal Plasma. *Ind. Eng. Chem. Res.* **2016**, *56*, 457–468.

(43) Li, S.; van Raak, T.; Gallucci, F. Investigating the operation parameters for ammonia synthesis in dielectric barrier discharge reactors. *J. Phys. D: Appl. Phys.* **2020**, *53*, 014008.

(44) Xie, Q.; Zhuge, S.; Song, X.; Lu, M.; Yu, F.; Ruan, R.; Nie, Y. Non-thermal atmospheric plasma synthesis of ammonia in a DBD reactor packed with various catalysts. *J. Phys. D: Appl. Phys.* **2020**, *53*, 064002.

(45) Moisan, M.; Nowakowska, H. Contribution of surface-wave (SW) sustained plasma columns to the modeling of RF and microwave discharges with new insight into some of their features. A survey of other types of SW discharges. *Plasma Sources Sci. Technol.* **2018**, *27*, 073001.

(46) Yamijala, S. S. R. K. C.; Nava, G.; Ali, Z. A.; Beretta, D.; Wong, B. M.; Mangolini, L. Harnessing Plasma Environments for Ammonia Catalysis: Mechanistic Insights from

Experiments and Large-Scale Ab Initio Molecular Dynamics. *J. Phys. Chem. Lett.* **2020**, *11*, 10469–10475.

(47) Uyama, H.; Matsumoto, O. Synthesis of Ammonia in High-Frequency Discharges. II. Synthesis of Ammonia in a Microwave Discharge Under Various Conditions. *Plasma Chem. Plasma Process.* **1989**, *9*, 421–432.

(48) Mingdong, B.; Xiyao, B.; Zhitao, Z.; Mindi, B. Synthesis of Ammonia in a Strong Electric Field Discharge at Ambient Pressure. *Plasma Chem. Plasma Process.* **2000**, *20*, 511–520.

(49) Mizushima, T.; Matsumoto, K.; Sugoh, J.; Ohkita, H.; Kakuta, N. Tubular membrane-like catalyst for reactor with dielectric-barrier-discharge plasma and its performance in ammonia synthesis. *Appl. Catal. A* **2004**, *265*, 53–59.

(50) Mizushima, T.; Matsumoto, K.; Ohkita, H.; Kakuta, N. Catalytic Effects of Metal-loaded Membrane-like Alumina Tubes on Ammonia Synthesis in Atmospheric Pressure Plasma by Dielectric Barrier Discharge. *Plasma Chem. Plasma Process.* **2007**, *27*, 1–11.

(51) Peng, P.; Li, Y.; Cheng, Y.; Deng, S.; Chen, P.; Ruan, R. Atmospheric Pressure Ammonia Synthesis Using Non-thermal Plasma Assisted Catalysis. *Plasma Chem Plasma Process.* **2016**, *36*, 1201–1210.

(52) Peng, P.; Cheng, Y.; Hatzenbeller, R.; Addy, M.; Zhou, N.; Schiappacasse, C.; Chen, D.; Zhang, Y.; Anderson, E.; Liu, Y.; Chen, P.; Ruan, R. Ru-based multifunctional mesoporous catalyst forlow-pressure and non-thermal plasma synthesis of ammonia. *Int. J. Hydrogen Energy* **2017**, *42*, 19056–19066.

(53) Kim, H.-H.; Teramoto, Y.; Ogata, A.; Takagi, H.; Nanba, T. Atmospheric-pressure nonthermal plasma synthesis of ammonia over ruthenium catalysts. *Plasma Processes Polym.* **2017**, *14*, 1–9.

(54) Body, T.; Cousens, S.; Kirby, J.; Corr, C. A volume-averaged model of nitrogen–hydrogen plasma chemistry to investigate ammonia production in a plasma-surface-interaction device. *Plasma Phys. Controlled Fusion* **2018**, *60*, 075011.

(55) Aihara, K.; Akiyama, M.; Deguchi, T.; Tanaka, M.; Hagiwara, R.; Iwamoto, M. Remarkable catalysis of a wool-like copper electrode for NH_3 synthesis from N_2 and H_2 in non-thermal atmospheric plasma. *Chem. Commun.* **2016**, *52*, 13560–13563.

(56) Kitano, M.; Inoue, Y.; Ishikawa, H.; Yamagata, K.; Nakao, T.; Tada, T.; Matsuishi, S.; Yokoyama, T.; Hara, M.; Hosono, H. Essential role of hydride ion in ruthenium-based ammonia synthesis catalysts. *Chem. Sci.* **2016**, *7*, 4036.

(57) Sharma, R. K.; Patel, H.; Mushtaq, U.; Kyriakou, V.; Zafeiropoulos, G.; Peeters, F.; Welzel, S.; van de Sanden, M. C. M.; Tsampas, M. N. Plasma Activated Electrochemical Ammonia Synthesis from Nitrogen and Water. *ACS Energy Letters* **2020**, *6*, 313–319.

(58) Peng, P.; Chen, P.; Schiappacasse, C.; Zhou, N.; Anderson, E.; Chen, D.; Liu, J.; Cheng, Y.; Hatzenbeller, R.; Addy, M.; Zhang, Y.; Liu, Y.; Ruan, R. A review on the non-thermal plasma-assisted ammonia synthesis technologies. *J. Cleaner Prod.* **2018**, *177*, 597–609.

(59) Sola, A.; Cotrino, J.; Gamero, A.; Colomer, V. Study of surface-wave-produced plasma column lengths. *J. Phys. D: Appl. Phys.* **1987**, *20*, 1250–1258.

(60) de Vries, N.; Palomares, J. M.; van Harskamp, W. J.; Iordanova, E. I.; Kroesen, G. M. W.; v d Mullen, J. J. A. M. Thomson scattering measurements on a low pressure surface wave sustained plasma in argon. *J. Phys. D: Appl. Phys.* **2008**, *41*, 105209.

(61) de Castro, A.; Alegre, D.; Tabarés, F. Influence of residence time and helium addition in the ammonia formation on tungsten walls in N_2-H_2 glow discharge plasmas. *Nucl. Mater. Energy* **2017**, *12*, 399–404.

(62) Winter, L. R.; Ashford, B.; Hong, J.; Murphy, A. B.; Chen, J. G. Identifying Surface Reaction Intermediates in Plasma Catalytic Ammonia Synthesis. *ACS Catal.* **2020**, 14763–14774.

(63) Hattori, M.; Iijima, S.; Nakao, T.; Hosono, H.; Hara, M. Solid solution for catalytic ammonia synthesis from nitrogen and hydrogen gases at 50°C. *Nat. Commun.* **2020**, *11*, 2001.

(64) Mehta, P.; Barboun, P. M.; Engelmann, Y.; Go, D. B.; Bogaerts, A.; Schneider, W. F.; Hicks, J. C. Plasma-Catalytic Ammonia Synthesis beyond the Equilibrium Limit. *ACS Catal.* **2020**, *10*, 6726–6734.

(65) Barboun, P.; Mehta, P.; Herrera, F. A.; Go, D. B.; Schneider, W. F.; Hicks, J. C. Distinguishing Plasma Contributions to Catalyst Performance in Plasma-Assisted Ammonia Synthesis. *ACS Sustainable Chem. Eng.* **2019**, *7*, 8621–8630.

(66) Kresse, G.; Furthmüller, J. Efficient iterative schemes for ab initio total-energy calculations using a plane-wave basis set. *Phys. Rev. B Condens. Matter* **1996**, *54*, 11169.

(67) Perdew, J. P.; Burke, K.; Ernzerhof, M. Generalized Gradient Approximation Made Simple. *Phys. Rev. Lett.* **1996**, *77*, 3865.

(68) Grimme, S.; Antony, J.; Ehrlich, S.; Krieg, H. A consistent and accurate ab initio parametrization of density functional dispersion correction (DFT-D) for the 94 elements H-Pu. *J. Chem. Phys.* **2010**, *132*, 154104.

(69) Blöchl, P. E. Projector augmented-wave method. *Phys. Rev. B* **1994**, *50*, 17953.

(70) Kresse, G.; Joubert, D. From ultrasoft pseudopotentials to the projector augmented-wave method. *Phys. Rev. B* **1999**, *59*, 1758.

(71) Abild-Pedersen, F.; Greeley, J.; Studt, F.; Rossmeisl, J.; Munter, T. R.; Moses, P. G.; Skúlason, E.; Bligaard, T.; Nørskov, J. K. Scaling Properties of Adsorption Energies for

Hydrogen-Containing Molecules on Transition-Metal Surfaces. *Phys. Rev. Lett.* **2007**, *99*.

(72) Peng, P.; Chen, P.; Addy, M.; Cheng, Y.; Anderson, E.; Zhou, N.; Schiappacasse, C.; Zhang, Y.; Chen, D.; Hatzenbeller, R.; Liu, Y.; Ruan, R. Atmospheric Plasma-Assisted Ammonia Synthesis Enhanced via Synergistic Catalytic Absorption. *ACS Sustainable Chem. Eng* **2019**, *7*, 100–104.

(73) Rouwenhorst, K. H. R.; Kim, H.-H.; Lefferts, L. Vibrationally Excited Activation of N_2 in Plasma-Enhanced Catalytic Ammonia Synthesis: A Kinetic Analysis. *ACS Sustanaible Chem. Eng.* **2019**, *7*, 17515–17522.

(74) Herrera, F. A.; Brown, G. H.; Barboun, P.; Turan, N.; Mehta, P.; Schneider, W. F.; Hicks, J. C.; Go, D. B. The impact of transition metal catalysts on macroscopic dielectric barrier discharge (DBD) characteristics in an ammonia synthesis plasma catalysis reactor. *J. Phys. D: Appl. Phys.* **2019**, *52*, 224002.

(75) Kim, H.-H.; Teramoto, Y.; Ogata, A.; Takagi, H.; Nanba, T. Plasma Catalysis for Environmental Treatment and Energy Applications. *Plasma Chem. Plasma Process.* **2015**, *36*, 45–72.

Graphical TOC Entry